Spatial Characterization of Multiple Pulses, With Different Spatial Profiles, From a Single Camera Snapshot

Ariel Veler, Michael Birk, Caleb Dobias, Rodrigo Amezcua Correa, Pavel Sidorenko, and Oren Cohen

***Abstract*—We used a single-shot ptychographic microscope to image the complex-valued (intensity and phase) spatial profiles of multiple ultrashort pulses. Specifically, we present a characterization of a burst of three ultrashort pulses with three nanoseconds delays between pulses using data recorded by a single camera exposure with millisecond integration time. This scheme is promising for various applications, including characterizing spatiotemporal mode-locked or Q-switched lasers, potentially shedding light on their buildup dynamics.**

***Index Terms*—Single shot multiplexed ptychography, beam characterization, ultrahigh speed imaging, microscopy, temporal resolution.**

I. Introduction

THE spatial characterization of an individual laser pulse in an isolated burst is an important task. It may reveal many physical processes, such as the build-up dynamic of spatiotemporal mode-locking [1] or resolve between entangled photons generated in distinct spatial modes of a fiber [2]. In the last decade, several methods for complete 3D field characterization were developed [3]. However, methods that can be implemented for imaging isolated bursts of pulses with varying spatial profiles typically suffer from relatively poor spatial resolution, complicated setups (often requiring a known reference pulse), and exhibit coupling between their spatial and temporal resolutions [3]. Thus, the characterization of an isolated, spatiotemporal pulse burst is still considered a challenging task.

Ptychography is a phase-sensitive microscopic imaging technique where a sample is scanned with a localized illuminating beam in a stepwise manner. At each scanning step, a far-field diffraction pattern is recorded [4]. Critically, the illumination spot in each step overlaps substantially with neighboring spots. Thus, the recorded information is highly redundant. The set of diffraction patterns is used for reconstructing the object's complex transfer function and the illuminating beam's complex spatial profile. The high degree of redundancy in the measured data allows ptychography for various forms of multiplexing, including wavelength multiplexing [5], [6] and temporal multiplexing [7], [8]. The ability to reconstruct the amplitude and phase of illumination by algorithmic demultiplexing makes ptychography very attractive for laser metrology. Indeed, wavelength multiplexing was used successfully for spatiospectral pulse characterization by broadband ptychography [9]. A significant and inherent limitation in conventional ptychography is the slow scanning process. To address this limitation, researchers have proposed and demonstrated single-shot ptychography (SSP) schemes [10], [11], [12]. In SSP, the object is illuminated by multiple beams

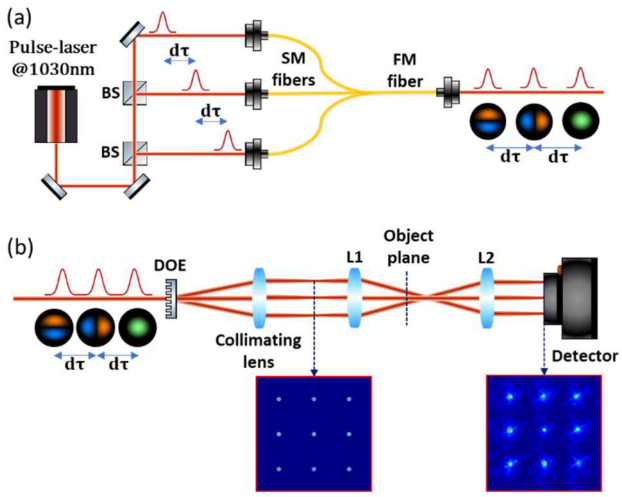

Fig. 1. Schematic diagrams of the burst generation and single-shot ptychographic microscope. (a) generation of a burst of laser pulses with different spatial profiles: Three pulses derived from the same source with a delay $d\tau$ between consecutive pulses enter into the single-mode side of a 3-mode photonic-lantern, and emerge through the few-mode side carrying the three fundamental modes, while maintaining the initial relative delays. (b) SSP microscope: the burst of pulses illuminates a DOE, gets collimated by a collimating lens, and then enters a 4f imaging system. A mask is located at the object plane near the Fourier plane of the 4f system. The field images present the intensity observed at the marked plane, by illuminating a Gaussian profile in the entrance plane.

Manuscript received 30 October 2023; revised 7 April 2024; accepted 19 April 2024. Date of publication 30 April 2024; date of current version 24 May 2024. This work was supported in part by the European Research Council (ERC) through the European Union's Horizon 2020 Research and Innovation Program under Grant 819440-TIMP, in part by the Army Research Office of Scientific Research under Grant W911NF1710553, and in part by NASA under Grant 80NSSC21K0624. *(Corresponding author: Oren Cohen.)*

Ariel Veler, Michael Birk, and Oren Cohen are with the Department of Physics and Solid State Institute, Technion, Haifa 32000, Israel (e-mail: arielv@campus.technion.ac.il; birkmichael@campus.technion.ac.il; oren@technion.ac.il).

Caleb Dobias and Rodrigo Amezcua Correa are with the CREOL, The College of Optics and Photonics, The University of Central Florida, Orlando, FL 32816 USA (e-mail: caleb.dobias@ucf.edu; r.amezcua@creol.ucf.edu).

Pavel Sidorenko is with the Department of Electrical and Computer Engineering and Solid State Institute, Technion, Haifa 32000, Israel (e-mail: sidorenko@technion.ac.il).

Digital Object Identifier 10.1109/JPHOT.2024.3392728

© 2024 The Authors. This work is licensed under a Creative Commons Attribution-NonCommercial-NoDerivatives 4.0 License. For more information, see https://creativecommons.org/licenses/by-nc-nd/4.0/

simultaneously and the whole ptychographic information is recorded in a single camera snapshot. An SSP system along with broadband ptychography was used for single-pulse, reference-free, spatiospectral pulse-beam characterization [13]. Moreover, an SSP system and broadband ptychography in conjunction with frequency-resolved optical gating [14] were used for complete, spatiotemporal characterization of femtosecond pulse. However, characterization of an isolated, i.e., not repeatable, burst of pulses has not been demonstrated yet.

Here, we demonstrate experimentally a ptychographic microscope that can resolve spatial profiles of individual pulses in a laser burst from a single camera snapshot, provided that these spatial profiles are different from each other. We reconstruct the complex-valued spatial profiles of three pulses, separated by 3 ns, from a recorded diffraction pattern by a camera with millisecond integration time (i.e., much longer than the pulse burst duration). Importantly, the spatial resolution of our microscope is decoupled from the temporal structure of the pulse burst. Additionally, the temporal resolution depends only on the pulses' overlap in time. The presented apparatus holds great promise for investigating the buildup dynamics of spatiotemporal mode-locked lasers.

II. Experimental Setup

In our experimental procedure, we begin by creating a burst of ultrashort pulses with complex spatiotemporal characteristics. Subsequently, we employ the SSP microscope to reconstruct the complex-valued spatial profiles of these pulses. To generate a spatiotemporally complex burst, we used a fiber-based Photonic Lantern (PL) [15], [16], [17], [18]. Our PL is composed of three Single-Mode (SM) fiber input channels, and a singular output channel, which is a Few-Mode (FM) fiber capable of supporting three fundamental modes of a step-index fiber. At the PL output, each SM input transforms into a distinct mode of the FM fiber in a one-to-one fashion. Fig. 1(a) shows the schematic setup that is used to generate the complex spatiotemporal burst. The pulse from the laser (Light Conversion, Pharos PH1) is split by two subsequent beam splitters into three replicas. Each replica is delayed by 3 ns relative to the previous replica, and coupled into a separate single-mode port of the PL. While the spectrum of the pulses can support a 180 fs duration, the pulses were chirped to 20 ps to avoid nonlinear spectral broadening and to prevent damage to the fibers. The output of the PL is a burst of three 20 ps pulses, temporally separated by 3 ns, copropagating along a single beamline. The spatial profile of each pulse resembles a different eigenmode of a step-index fiber (Fig. 1(a)).

This spatiotemporally complex burst is then measured using a 4f system-based SSP microscope (4fSSP) [10], [19] (Fig. 1(b)). The SSP microscope consists of a two-dimensional diffractive optical element (DOE) [20], a collimating lens, and a 4f system. The DOE (MS-817-J-Y-A, Holo-Or Ltd.) is placed at the entrance of the optical system and is used to divide the incoming beam into 5X5 identical replicas, each representing a different diffraction order $\{-2,\ -1,\ 0,\ 1,\ 2\}$ along both the vertical and horizontal axes. The replicas have a separation angle $\theta_s = 0.97^\circ$. The collimating lens with focal length $f_{col} = 150\,\text{mm}$ is located f_{col} after the DOE, ensuring that all beam replicas are effectively parallel when entering the 4f system. The spacing between the centers of neighboring beams on the horizontal and vertical axes at the entrance plane to the 4f system is determined by $b = \tan(0.97)*150 = 2.54\text{mm}$. The input plane of the 4f system coincides with the back focal plane of the collimating lens. Within the 4f system, the focal lengths of the two lenses, L1 and L2, were $f_1 = 100\,\text{mm}$ and $f_2 = 60\,\text{mm}$, respectively. Lens L1 focuses the beam replicas toward a known object. The object is located at a small distance $d = 15\,\text{mm}$ before the Fourier plane of the 4f system. This arrangement ensures that the neighboring replicas illuminate different, yet partially overlapping areas of the object, with an overlap of approximately 66% (for calculation details, see Appendix A). Lens L2 transforms the field that was diffracted by the object into k-space. The camera, which is located at the output plane of the 4f system records the intensity pattern (IDS UI-3200-M-GL, with 3006x4104 pixels, pixel size of $3.45\mu\,\text{m}$ and 12-bit dynamic range). The object's spatial power spectrum is confined, thus the resulting pattern observed at the camera exhibits clearly discernible blocks [10]. Each block holds an individual diffraction pattern associated with a specific replica, and contains information about the corresponding region of the object illuminated by that replica.

In our experiment, we aim at the characterization of the burst. The pattern recorded in a single camera snapshot represents the incoherent sum of intensity patterns (i.e., multiplexed diffraction patterns), with each pattern originating from an individual pulse within the burst. That is, the intensity diffraction pattern of each block on the camera is described by:

$$I_m(\boldsymbol{\nu}) = \sum_{k=1}^{3} \left| F\left[P_k(\boldsymbol{r} - \boldsymbol{R}_m)O(\boldsymbol{r})\right]\right|^2 \tag{1}$$

When $\boldsymbol{\nu}$ and $\boldsymbol{r}$ are the spatial coordinates in the camera and object planes, respectively, $m = 1, \ldots, 25$ is the block index, $\mathrm{k} = 1, 2, 3$ is the pulse index in the burst, R_m is the location of replica m on the object plane, F is the 2D Fourier operator, I is the measured intensity pattern and $P,\ O$ correspond to the complex distributions of the probes and object, respectively.

III. Reconstruction Process

We aim to algorithmically reconstruct the three probes' complex distributions, i.e., $P_k(\boldsymbol{r})$, from the single intensity pattern $I(\boldsymbol{\nu})$ which is presented in Fig. 2(a). For calibration, we obtained two reference images: one without the mask to establish the positions of the beams' centers on the object plane, and another without any laser illumination for background noise reduction using the method described in [21]. We have found that applying a threshold on the minimum values after subtracting the background was an essential step in preventing artifacts in the reconstruction procedure.

To reconstruct the spatial profile of the three pulses, we first characterized the mask. To do this, we illuminate the mask using only a single pulse, such that our system is identical to the SSP microscope [10]. The detailed acquisition process is provided in Appendix B. We reconstruct the complex-valued transmission function of the mask by applying 500 iterations of the ePIE algorithm [22] (Fig. 2(b)). This mask reconstruction was employed as the known object in the Multi-state Ptychographic Algorithm

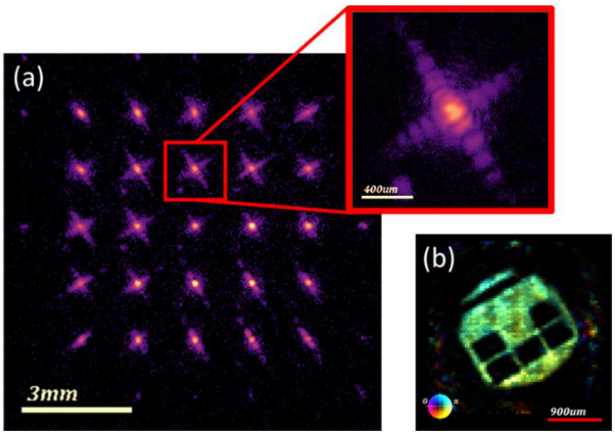

Fig. 2. (a) Recorded intensity pattern of the three pulses accumulated on the camera. The inset image is a close-up of one of the blocks. (b) Reconstruction of the mask from the SSP microscope. This recovery is used as a constant object in the MsPA algorithm for the reconstruction of the three probes.

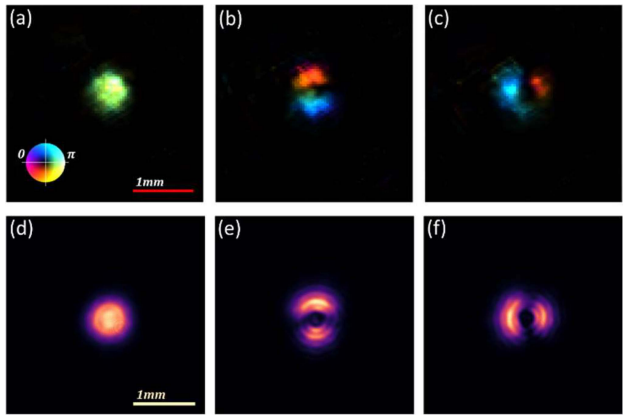

Fig. 3. Experimental demonstration of single-shot burst characterization. (a)–(c) The complex-valued spatial profiles of the pulses in the burst reconstructed from the diffraction pattern in Fig. 2(a). In these images, colors present relative phases. (d)–(f) For comparison, independently measured intensity spatial profiles of the probes.

(MsPA) [5] (we verified numerically that the used mask is not unique and that other masks yield similar performances). For good reconstructions, the power spectrum of the mask should correspond to the power spectra of the probed spatial profiles.

Next, we illuminate the microscope with the spatiotemporal burst and record the multiplexed diffraction pattern (Fig. 2(a)). The recorded intensity pattern is divided into 25 blocks around the calculated centers, and used as input for the MsPA algorithm [5]. In addition to the diffraction data, the algorithm requires as an input initial guesses for the probes and for the object. Here, we utilized a modified version of the algorithm, where the fixed, known mask represents the object and is not updated by the algorithm (full diagram in Fig. 4 in Appendix C). The focus of the reconstruction process was solely on the unknown probes. As for initial guesses, all that was required from the probes' guesses was that they were not identical, to avoid degeneracy in the reconstruction process. To this end, we opted for simple linear functions $val(x, y) = ax + by + c$ with different values of a, b, c for each guess (other initial guesses were tested numerically and yielded similar results). We performed 500 iterations over the data, allowing only the probes to be updated. The restored spatial profiles of the probes were already clear after 50 iterations, but we continued up to 500 iterations to ensure convergence.

We note that the reconstruction procedure assumes that the spatial profiles of the pulses are different from each other. If pulses have the same profile, a single pulse with this profile will be reconstructed. While for noiseless data it is enough that the spatial profiles are not identical [23], they should differ sufficiently when the data is noisy.

IV. Results

We reconstruct the complex-valued spatial profiles of the pulses in the burst by applying the reconstruction algorithm to the recorded data shown in Fig. 2(a). Fig. 3(a)–(c) present the reconstruction of the complex-valued (intensity and phase) spatial profile of the intra-burst pulses, when they illuminate the object plane. The reconstructions present a good similarity to the three complex-valued fundamental modes of a step-index fiber, as was expected from the FM fiber of the PL device. For comparison, we show the intensity profiles of the three probes that were captured by placing the detector at the object plane and imaging one pulse per exposure (without the object and DOE) in Fig. 3(d)–(f). Clearly, there is a good match between the measured intensity profiles and the complex-valued reconstructed profiles. A numerical investigation of the reconstruction in the presence of noise is described in Appendix D and Fig. 5.

V. Conclusion

This study demonstrated the reconstruction of the complex-valued spatial profiles of multiple, non-repetitive pulses within a single burst. We reconstructed the profiles of three pulses from a single camera snapshot. Importantly the spatial resolution of our microscope is completely decoupled from the temporal structure of the pulse burst. A key requirement is that the pulses are well separated from each other such that they do not interfere on the detector. The presented technique offers exciting potential for various applications, including exploring the buildup dynamics in spatiotemporal mode-locked lasers and investigating spatial pattern bistabilities within laser systems [24].

Appendix A
Overlap Integral Calculation

To determine the optimal location for the object plane, which is displaced by distance d from the Fourier plane of the 4f system (see Fig. 1(b)), we calculated the overlap integral between two neighboring beams. We assume a Gaussian beam profile (a good approximation for the first mode of the PL). The width of each beam is W (1/e from maximum amplitude, half width). The space between adjacent beams' centers is R. The overlap integral is:

$$S(W,R) = \frac{1}{\sqrt{\pi W^2}} \int_{-\infty}^{\infty} \min \left[e^{-\left(\frac{x+\frac{R}{2}}{W}\right)^2}, e^{-\left(\frac{x-\frac{R}{2}}{W}\right)^2} \right] dx$$

$$= \frac{2}{\sqrt{\pi W^2}} \int_0^{\infty} e^{-\left(\frac{x+\frac{R}{2}}{W}\right)^2} dx$$

$$S(W,R) = Erfc\left(\frac{R}{2W}\right) \tag{2}$$

In our experiment, the width of the beam at the entrance plane of the system was measured to be $W_0 = 0.925[mm]$, which yielded a width of the beams on the object plane of $W_{obj} = W_0 \cdot (\frac{f_1}{f_{col}}) = 0.617$[mm]. The distance between neighboring beams in the object plane was $R = \frac{(b \cdot d)}{f_1} = \frac{2.54 \cdot 15}{100} = 0.381$[mm]. For the case of a Gaussian beam, the overlap between adjacent probes was $Erfc(\frac{0.381}{2 \cdot 0.617}) \cong 66\%$.

Appendix B
Object Characterization Procedure

To start, we removed the DOE and the mask, positioned the camera at the mask plane, and recorded images of the probes' intensities at this plane, each probe in turn (see Fig. 3(d)–(f)). Next, we reinstated the system to its original state, and obtained a high dynamic range (HDR) image by repeatedly applying the third probe (the last one in the pulse burst) with various camera exposures. We used the recorded probe image as an initial guess for the probe function (Fig. 3(f)), and applied the ePIE algorithm as described.

Appendix C
Revised MsPA Algorithm

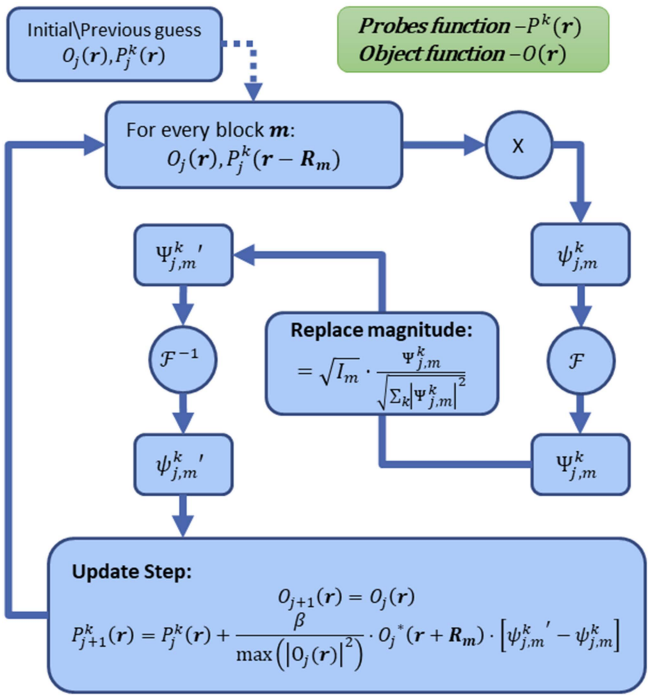

Fig. 4. Diagram of the reconstruction algorithm. The algorithm is identical to the standard MsPA algorithm, except for not restoring the object, which remains constant over the entire process. A complete iteration corresponds to applying the process presented in the diagram to all diffraction image blocks.

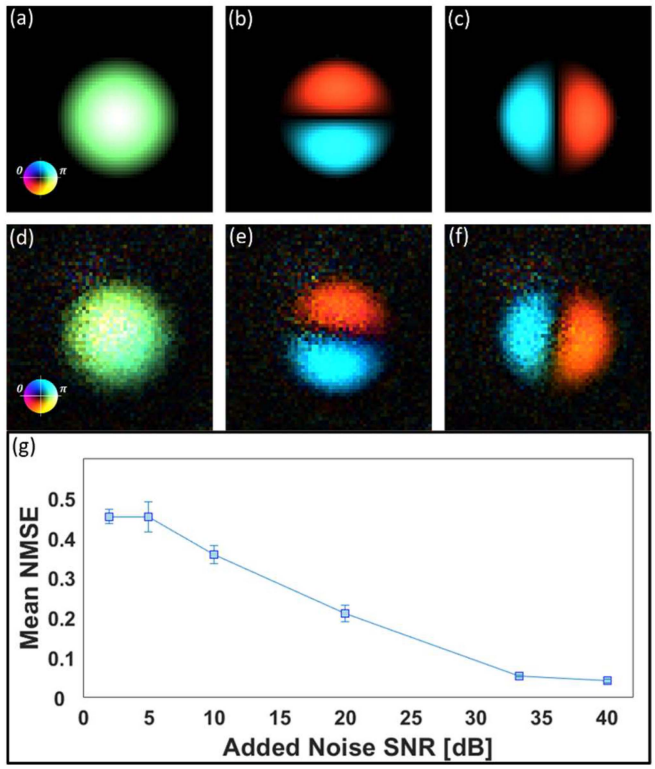

Fig. 5. Reconstructions (same as in Fig. 3) of numerical data. (a)–(c) without noise, (d)–(f) with 33.3[dB] SNR. (g) Mean NMSE of the three probes reconstructions as a function of SNR.

Appendix D
Numerical Investigation of Reconstruction As a Function of SNR

Fig. 5 presents reconstructions (similar to Fig. 3 in the main text) of data produced numerically for various SNR levels (white Gaussian noise was added to the intensity) [25]. The PSNR in the experiment (after background reduction) is $\sim 33.3[dB]$. These results support the validity of the reconstruction of the experimental data (Fig. 3).

References

[1] L. G. Wright, D. N. Christodoulides, and F. W. Wise, "Spatiotemporal mode-locking in multimode fiber lasers," *Science*, vol. 358, no. 6359, pp. 94–97, Oct. 2017, doi: 10.1126/science.aao0831.
[2] K. Sulimany and Y. Bromberg, "All-fiber source and sorter for multimode correlated photons," *npj Quantum Inf*, vol. 8, no. 1, Jan. 2022, Art. no. 4, doi: 10.1038/s41534-021-00515-x.
[3] S. W. Jolly, O. Gobert, and F. Quéré, "Spatio-temporal characterization of ultrashort laser beams: A tutorial," *J. Opt.*, vol. 22, no. 10, Oct. 2020, doi: 10.1088/2040-8986/abad08.
[4] J. M. Rodenburg, "Ptychography and related diffractive imaging methods," *Adv. Imag. Electron Phys.*, vol. 150, pp. 87–184, 2008, doi: 10.1016/S1076-5670(07)00003-1.
[5] P. Thibault and A. Menzel, "Reconstructing state mixtures from diffraction measurements," *Nature*, vol. 494, no. 7435, pp. 68–71, Feb. 2013, doi: 10.1038/nature11806.
[6] D. J. Batey, D. Claus, and J. M. Rodenburg, "Information multiplexing in ptychography," *Ultramicroscopy*, vol. 138, pp. 13–21, Mar. 2014, doi: 10.1016/j.ultramic.2013.12.003.

[7] P. Sidorenko, O. Lahav, and O. Cohen, "Ptychographic ultrahigh-speed imaging," *Opt. Exp.*, vol. 25, no. 10, pp. 10997–11008, May 2017, doi: 10.1364/OE.25.010997.

[8] O. Wengrowicz et al., "Experimental time-resolved imaging by multiplexed ptychography," *Opt. Exp.*, vol. 27, no. 17, pp. 24568–24577, Aug. 2019, doi: 10.1364/OE.27.024568.

[9] D. Goldberger, D. Schmidt, J. Barolak, B. Ivanic, C. G. Durfee, and D. E. Adams, "Spatiospectral characterization of ultrafast pulse-beams by multiplexed broadband ptychography," *Opt. Exp.*, vol. 29, no. 20, pp. 32474–32490, Sep. 2021, doi: 10.1364/OE.433752.

[10] P. Sidorenko and O. Cohen, "Single-shot ptychography," *Optica*, vol. 3, no. 1, pp. 9–14, Jan. 2016, doi: 10.1364/OPTICA.3.000009.

[11] X. Pan, C. Liu, and J. Zhu, "Single shot ptychographical iterative engine based on multi-beam illumination," *Appl. Phys. Lett.*, vol. 103, no. 17, Oct. 2013, Art. no. 171105, doi: 10.1063/1.4826273.

[12] D. Goldberger, J. Barolak, C. G. Durfee, and D. E. Adams, "Three-dimensional single-shot ptychography," *Opt. Exp.*, vol. 28, no. 13, pp. 18887–18898, Jun. 2020, doi: 10.1364/OE.395205.

[13] D. Goldberger et al., "Single-pulse, reference-free, spatiospectral measurement of ultrashort pulse-beams," *Optica*, vol. 9, no. 8, pp. 894–902, Aug. 2022, doi: 10.1364/OPTICA.462586.

[14] D. Goldberger et al., "Single-pulse, reference-free, spatiotemporal characterization of ultrafast laser pulse beams via broadband ptychography," *Opt. Lett.*, vol. 48, no. 13, pp. 3455–3458, Jul. 2023, doi: 10.1364/OL.493234.

[15] S. G. Leon-Saval, T. A. Birks, J. Bland-Hawthorn, and M. Englund, "Multimode fiber devices with single-mode performance," *Opt. Lett.*, vol. 30, no. 19, pp. 2545–2547, Oct. 2005, doi: 10.1364/OL.30.002545.

[16] A. M. Velazquez-Benitez et al., "Six mode selective fiber optic spatial multiplexer," *Opt. Lett.*, vol. 40, no. 8, pp. 1663–1666, Apr. 2015, doi: 10.1364/OL.40.001663.

[17] S. G. Leon-Saval, N. K. Fontaine, and R. Amezcua-Correa, "Photonic lantern as mode multiplexer for multimode optical communications," *Opt. Fiber Technol.*, vol. 35, pp. 46–55, Feb. 2017, doi: 10.1016/j.yofte.2016.08.005.

[18] D. Cruz-Delgado, S. Yerolatsitis, N. K. Fontaine, D. N. Christodoulides, R. Amezcua-Correa, and M. A. Bandres, "Synthesis of ultrafast wavepackets with tailored spatiotemporal properties," *Nature Photon.*, vol. 16, pp. 686–691, Aug. 2022, doi: 10.1038/s41566-022-01055-2.

[19] A. Veler, M. Birk, C. Dobias, R. A. Correa, P. Sidorenko, and O. Cohen, "Single-shot ptychographic imaging of non-repetitive ultrafast events," *Opt. Lett.*, vol. 49, no. 2, pp. 178–181, Jan. 2024, doi: 10.1364/OL.502848.

[20] S. Katz, N. Kaplan, and I. Grossinger, "Using diffractive optical elements: DOEs for beam shaping - fundamentals and applications," *Optik Photonik*, vol. 13, no. 4, pp. 83–86, Nov. 2018, doi: 10.1002/opph.201870416.

[21] C. Wang, Z. Xu, H. Liu, Y. Wang, J. Wang, and R. Tai, "Background noise removal in X-ray ptychography," *Appl. Opt.*, vol. 56, no. 8, pp. 2099–2111, Mar. 2017, doi: 10.1364/AO.56.002099.

[22] A. M. Maiden and J. M. Rodenburg, "An improved ptychographical phase retrieval algorithm for diffractive imaging," *Ultramicroscopy*, vol. 109, no. 10, pp. 1256–1262, Sep. 2009, doi: 10.1016/j.ultramic.2009.05.012.

[23] P. Li, T. Edo, D. Batey, J. Rodenburg, and A. Maiden, "Breaking ambiguities in mixed state ptychography," *Opt. Exp.*, vol. 24, no. 8, pp. 9038–9052, Apr. 2016, doi: 10.1364/oe.24.009038.

[24] C. Tamm and C. O. Weiss, "Bistability and optical switching of spatial patterns in a laser," *J. Opt. Soc. Amer. B.*, vol. 7, no. 6, pp. 1034–1038, Jun. 1990, doi: 10.1364/JOSAB.7.001034.

[25] P. Lou, S. P. Veetil, X. He, A. Sun, S. Wang, and C. Liu, "Analytical linear model for fourier ptychography: Insights into image uniqueness and reconstruction factors," *Opt. Eng.*, vol. 63, no. 3, Mar. 2024, Art. no. 033103, doi: 10.1117/1.OE.63.3.033103.